MFBE_2001: COMPUTATION OF MAGNETIC FIELDS OF IDEAL MHD EQUILIBRIA

E. Strumberger, P. Merkel, E. Schwarz and C. Tichmann

Max-Planck-Institut für Plasmaphysik, IPP-Euratom Association
85748 Garching, Germany

IPP Report 5/100 **May 2002**

TABLE OF CONTENTS

ABSTRACT

Using the 'virtual casing' principle the parallel MFBE_2001 code computes the magnetic field of three-dimensional ideal MHD equilibria in a form suitable for tracing field lines and guiding centres. This report gives a detailed description of theory, numerical methods and use of MFBE_2001. Examples for tokamak, currentless stellarator and quasi-axisymmetric stellarator configurations demonstrate its multi-purpose applicabilities.

1. INTRODUCTION

Originally, the MFBE (**M**agnetic Field Solver for **F**inite-**B**eta **E**quilibria) code [1] was developed for computing magnetic fields in a form suitable for field line tracing inside and outside the plasma boundary of three-dimensional ideal MHD equilibria of stellarators without net toroidal current, e.g. Wendelstein 7-X (W7-X) [2]. That code version, which takes advantage of the stellarator symmetry, uses the single-valued magnetic potential Φ computed by the free-boundary equilibrium code NEMEC [3] to determine the vacuum field $\mathbf{B}_\mathrm{v}$ of the equilibrium

$$\mathbf{B}_\mathrm{v} = \mathbf{B}_\mathrm{c} + \nabla\Phi, \tag{1}$$

with $\mathbf{B}_\mathrm{c}$ being the magnetic field produced by external coils. This relation only holds in the case of vanishing net toroidal current. For equilibria with net toroidal current, such as quasi-axisymmetric or tokamak equilibria, the magnetic field produced by this current has to be added. A more elegant way to compute $\mathbf{B}_\mathrm{v}$ for equilibria with and without net toroidal current is the 'virtual casing' principle [4]. The new MFBE code named MFBE_2001 is based on this principle, and it has been extended to asymmetric configurations.

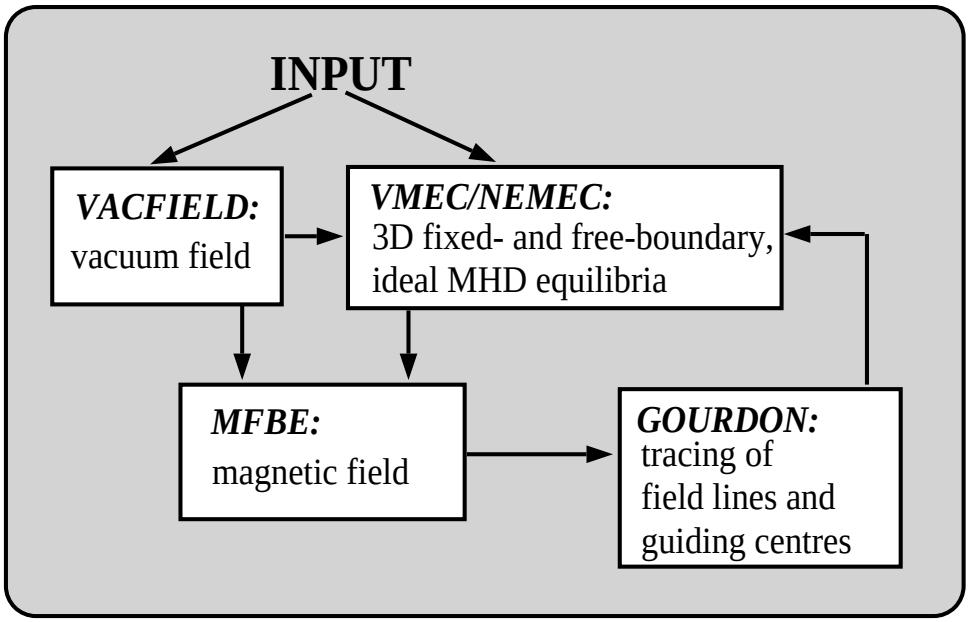

Fig. 1: Overview of the code system

MFBE_2001 is part of a code system illustrated in Fig. 1. The VACFIELD code computes the magnetic field $\mathbf{B}_\mathrm{c}$ of external coil currents (e.g. toroidal coils, poloidal coils, modular coils, ...) by means of Biot-Savart's law. It needs as input the coil geometry and the coil currents. Assuming nested flux surfaces, fixed or free-boundary three-dimensional

equilibria are computed with the VMEC/NEMEC code for given pressure and rotational transform profiles or pressure and toroidal current profiles. The fixed-boundary VMEC code [3, 5] needs the geometry of the plasma boundary, while an initial guess of this boundary and the external magnetic field $\mathbf{B}_c$ have to be provided for the free-boundary NEMEC code [3]. Then MFBE_2001 calculates the corresponding magnetic field inside and outside the plasma boundary in a form suitable for the GOURDON code which traces field lines and guiding centres.

The main applications of this code system are:

Iterative procedure for determining the last closed magnetic surface (LCMS):

The VMEC/NEMEC code assumes nested flux surfaces, that is, it yields solutions with closed flux surfaces even if islands or ergodic regions exist. In order to compute a free-boundary equilibrium with a boundary that coincides with the last closed magnetic surface of the corresponding magnetic field, the code system NEMEC+MFBE+GOURDON has to be used. In the free-boundary NEMEC code the total toroidal flux serves as free parameter to adjust the aspect ratio of an ideal MHD equilibrium for a given external field $\mathbf{B}_c$. With NEMEC+MFBE+GOURDON this parameter is determined iteratively. For this purpose, equilibria are computed with NEMEC for various values of the total toroidal flux. The corresponding magnetic fields inside and outside the plasma boundary are calculated with MFBE_2001 and their last closed magnetic surfaces are determined by field line tracing using the GOURDON code. If the plasma boundary of the equilibrium lies completely inside the LCMS, the toroidal flux is to small. Then the flux is increased until the equilibrium plasma boundary coincides with the LCMS of the corresponding magnetic field. For more details see Chapter 5 and Ref. [1].

Investigation of the magnetic field structure

Properties of the magnetic field are studied with the GOURDON code by field line tracing. Interesting points are, for example, size and position of macroscopic islands outside the plasma boundary [6] and the ergodization of the edge region [7, 8].

Divertor studies

Tracing field lines and guiding centres, the deposition patterns of field lines and particles on plasma-facing components (PFC's), e.g. divertor and baffle plates, first wall, etc., are determined and a rough estimate of the power load on these structures becomes possible [9, 10, 11].

2. THEORY

2.1 EQUILIBRIUM COMPUTATION

The VMEC/NEMEC code has been extended from stellarator-symmetric equilibria to asymmetric equilibria by S.P. Hirshman. Here some details of this upgraded code version which are necessary for the understanding of MFBE_2001 are described.

The three-dimensional VMEC code [3, 5] is a fixed-boundary equilibrium code assuming nested flux surfaces. Its basic goal is to minimize the total energy W_p (magnetic plus thermal) of a plasma confined in a toroidal domain V_p.

$$W_\mathrm{p} = \int_{V_\mathrm{p}} \left(\frac{1}{2} \frac{B^2}{\mu_0} + p \right) dV \tag{2}$$

VMEC uses the left-handed curvilinear coordinates (s, θ, ζ) with the radial coordinate s being the normalized toroidal flux, the poloidal coordinate θ $(0 \leq \theta < 2\pi)$ and the toroidal coordinate ζ $(0 \leq \zeta < 2\pi)$. These coordinates are related with the cylindrical coordinates (R, φ, Z)

$$R = \sum_{\mathrm{m}=0,\mathrm{n}=-\mathrm{n_b}}^{\mathrm{m_b},\mathrm{n_b}} \hat{r}^{\mathrm{c}}_{\mathrm{m,n}}(s)\cos(\mathrm{m}\theta - \mathrm{n}\zeta\mathrm{N_p}) + \hat{r}^{\mathrm{s}}_{\mathrm{m,n}}(s)\sin(\mathrm{m}\theta - \mathrm{n}\zeta\mathrm{N_p})$$

$$\varphi = \zeta \tag{3}$$

$$Z = \sum_{\mathrm{m}=0,\mathrm{n}=-\mathrm{n_b}}^{\mathrm{m_b},\mathrm{n_b}} \hat{z}^{\mathrm{c}}_{\mathrm{m,n}}(s)\cos(\mathrm{m}\theta - \mathrm{n}\zeta\mathrm{N_p}) + \hat{z}^{\mathrm{s}}_{\mathrm{m,n}}(s)\sin(\mathrm{m}\theta - \mathrm{n}\zeta\mathrm{N_p})$$

with $\{\hat{r}^{\mathrm{c}}_{\mathrm{m,n}}(s), \hat{r}^{\mathrm{s}}_{\mathrm{m,n}}(s), \hat{z}^{\mathrm{c}}_{\mathrm{m,n}}(s), \hat{z}^{\mathrm{s}}_{\mathrm{m,n}}(s)\}$ being the Fourier coefficients of a flux surface with normalized toroidal flux s. $\mathrm{N_p}$ is the number of periods, $0 \leq \mathrm{m} \leq \mathrm{m_b}$ are the poloidal mode numbers and $-\mathrm{n_b} \leq \mathrm{n} \leq \mathrm{n_b}$ are the toroidal mode numbers. The contravariant components of the magnetic field are

$$B^s = 0$$

$$B^\theta = \sum_{\mathrm{m}=0,\mathrm{n}=-\mathrm{n_b}}^{\mathrm{m_b},\mathrm{n_b}} \hat{b}^{\theta,\mathrm{c}}_{\mathrm{m,n}}(s)\cos(\mathrm{m}\theta - \mathrm{n}\zeta\mathrm{N_p}) + \hat{b}^{\theta,\mathrm{s}}_{\mathrm{m,n}}(s)\sin(\mathrm{m}\theta - \mathrm{n}\zeta\mathrm{N_p}) \tag{4}$$

$$B^\zeta = \sum_{\mathrm{m}=0,\mathrm{n}=-\mathrm{n_b}}^{\mathrm{m_b},\mathrm{n_b}} \hat{b}^{\zeta,\mathrm{c}}_{\mathrm{m,n}}(s)\cos(\mathrm{m}\theta - \mathrm{n}\zeta\mathrm{N_p}) + \hat{b}^{\zeta,\mathrm{s}}_{\mathrm{m,n}}(s)\sin(\mathrm{m}\theta - \mathrm{n}\zeta\mathrm{N_p})$$

with the Fourier coefficients $\{\hat{b}^{\theta,\mathrm{c}}_{\mathrm{m,n}}(s), \hat{b}^{\theta,\mathrm{s}}_{\mathrm{m,n}}(s), \hat{b}^{\zeta,\mathrm{c}}_{\mathrm{m,n}}(s), \hat{b}^{\zeta,\mathrm{s}}_{\mathrm{m,n}}(s)\}$.

VMEC yields the Fourier coefficients $\{\hat{r}^{\mathrm{c}}_{\mathrm{m,n}}(s_{\mathrm{i}}), \hat{r}^{\mathrm{s}}_{\mathrm{m,n}}(s_{\mathrm{i}}), \hat{z}^{\mathrm{c}}_{\mathrm{m,n}}(s_{\mathrm{i}}), \hat{z}^{\mathrm{s}}_{\mathrm{m,n}}(s_{\mathrm{i}})\}$ of a discrete number of nested flux surfaces i with $1 \leq \mathrm{i} \leq \mathrm{N}_s$ and the Fourier coefficients $\{\hat{b}^{\theta,\mathrm{c}}_{\mathrm{m,n}}(s_{\mathrm{j}}), \hat{b}^{\theta,\mathrm{s}}_{\mathrm{m,n}}(s_{\mathrm{j}}), \hat{b}^{\zeta,\mathrm{c}}_{\mathrm{m,n}}(s_{\mathrm{j}}), \hat{b}^{\zeta,\mathrm{s}}_{\mathrm{m,n}}(s_{\mathrm{j}})\}$ of the corresponding magnetic field on flux surfaces in between, that is, $s_{\mathrm{j}} = (s_{\mathrm{i}} + s_{\mathrm{i+1}})/2$ (for details see Fig. 2).

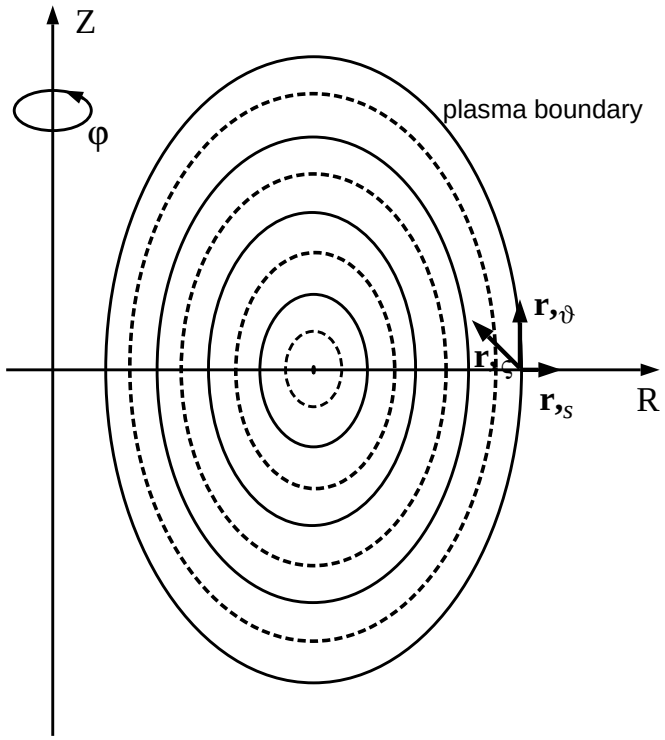

Fig. 2: Flux surfaces from the magnetic axis to the plasma boundary for a toroidal cross-section in a cylindrical coordinate system (R, φ, Z). The solid lines mark the flux surfaces on which the Fourier coefficients $\{\hat{r}^{\mathrm{c}}_{\mathrm{m,n}}(s_{\mathrm{i}}), \hat{r}^{\mathrm{s}}_{\mathrm{m,n}}(s_{\mathrm{i}}), \hat{z}^{\mathrm{c}}_{\mathrm{m,n}}(s_{\mathrm{i}}), \hat{z}^{\mathrm{s}}_{\mathrm{m,n}}(s_{\mathrm{i}})\}$ are given, while the dashed lines belong to surfaces on which the Fourier coefficients of the magnetic field are defined. The arrows represent the curvilinear basis vectors $(\mathbf{r}_{,s}\,, \mathbf{r}_{,\theta}\,, \mathbf{r}_{,\zeta})$.

The three-dimensional free-boundary NEMEC code [3] is a synthesis of the VMEC code and the NESTOR vacuum code [12]. There, the shape of the plasma boundary is determined by the pressure balance

$$\frac{1}{2}\frac{B^2_{\mathrm{p}}}{\mu_0} + p = \frac{1}{2}\frac{B^2_{\mathrm{v}}}{\mu_0} \tag{5}$$

with vanishing normal component of the magnetic field at the boundary.

$$\mathbf{B}_{\mathrm{v}} \cdot \mathbf{n} = (\mathbf{B}_{\mathrm{c}} + \nabla\Phi) \cdot \mathbf{n} = 0 \tag{6}$$

Here $\mathbf{B}_{\mathrm{p}}$ is the magnetic field inside the plasma boundary, p is the plasma pressure and $\mathbf{n}$ is the normal unit vector external-perpendicular to the plasma boundary. Note, considering

equilibria with net toroidal current I, the corresponding magnetic field $\mathbf{B}_I$ has to be added in Eq. (6).

$$\mathbf{B}_\mathrm{v} \cdot \mathbf{n} = (\mathbf{B}_\mathrm{c} + \nabla\Phi + \mathbf{B}_I) \cdot \mathbf{n} = 0 \tag{7}$$

NESTOR solves the Neumann boundary value problem yielding the single-valued magnetic potential Φ. It computes the value $B_\mathrm{v}^2/2\mu_0$ at the plasma boundary which is the only outside quantity required to determine the free-boundary equilibrium, while $\mathbf{B}_\mathrm{p}$, p and I are determined by the VMEC code. The equilibrium vacuum field $\mathbf{B}_\mathrm{v}$ and the corresponding free plasma boundary are obtained by iterating the position of the free boundary with a constant toroidal flux enclosed.

2.2 THE 'VIRTUAL-CASING' PRINCIPLE

The magnetic field $\mathbf{B}$ of a MHD equilibrium is a superposition of the external magnetic field $\mathbf{B}_\mathrm{c}$ and the field of the plasma currents $\mathbf{B}_\mathrm{j}$.

$$\mathbf{B} = \mathbf{B}_\mathrm{c} + \mathbf{B}_\mathrm{j} \tag{8}$$

Inside the plasma boundary $\mathbf{B} = \mathbf{B}_\mathrm{p}$ is known from the solution of an equilibrium computation, e.g. performed with the VMEC or NEMEC code. Outside this boundary it is possible to determine $\mathbf{B} = \mathbf{B}_\mathrm{v}$ by using the 'virtual-casing' principle [4]. It assumes that the considered equilibrium configuration is surrounded by a closed superconducting sheath S coinciding with the plasma boundary. Outside this sheath the magnetic field will be zero. Then the only magnetic field sources are the plasma currents and the surface current $\mathbf{j}_S$ induced in the superconductor.

$$\mathbf{j}_S = \frac{1}{\mu_0}\mathbf{B}_S \times \mathbf{n} \tag{9}$$

Here $\mathbf{B}_S$ is the equilibrium magnetic field on the surface S and $\mathbf{n}$ is the normal unit vector external-perpendicular to this surface. This current creates $\mathbf{B}_\mathrm{c}$ in the internal region,

$$\mathbf{B}_\mathrm{c} = \frac{\mu_0}{4\pi}\int_S df' \frac{\mathbf{j}'_S \times (\mathbf{r} - \mathbf{r}')}{|\mathbf{r} - \mathbf{r}'|^3} \tag{10}$$

with the positions $\mathbf{r}'$ on the sheath S and $\mathbf{r}$ lying in the plasma region. In the external region the current $\mathbf{j}_S$ creates a magnetic field which is equal in magnitude and opposite in sign to the field produced by the current flowing in the plasma, that is,

$$\mathbf{B}_\mathrm{j} = -\frac{\mu_0}{4\pi}\int_S df' \frac{\mathbf{j}'_S \times (\mathbf{r} - \mathbf{r}')}{|\mathbf{r} - \mathbf{r}'|^3} \tag{11}$$

with $\mathbf{r}$ lying in the external region.

The definitions of the curvilinear coordinates (s, v, u) and the explicit formulation of the equations used in MFBE_2001 are described in detail in the next section.

3. NUMERICAL DETAILS OF MFBE_2001

3.1 DEFINITION OF THE GRID

For tracing field lines or guiding centres the magnetic field has to be calculated many times. The number of calculations of the magnetic field is considerably reduced by computing it on a grid from which the required values are interpolated. This grid has to cover the relevant region and it has to be sufficiently fine to guarantee results independent of its discreteness. The grid box plotted in Fig. 3 is chosen as cylindrical box satisfying the first requirement. The box is centred around the coordinates (R_0, Z_0). The half side lengths of the box are given by ΔR and ΔZ. Since R_0, Z_0, ΔR and ΔZ do not vary in toroidal direction, it has to be made sure that the box fits for all toroidal cross-sections in case of three-dimensional configurations. To satisfy the second requirement the box has to be divided into a sufficient number of grid points N_R, N_φ and N_Z.

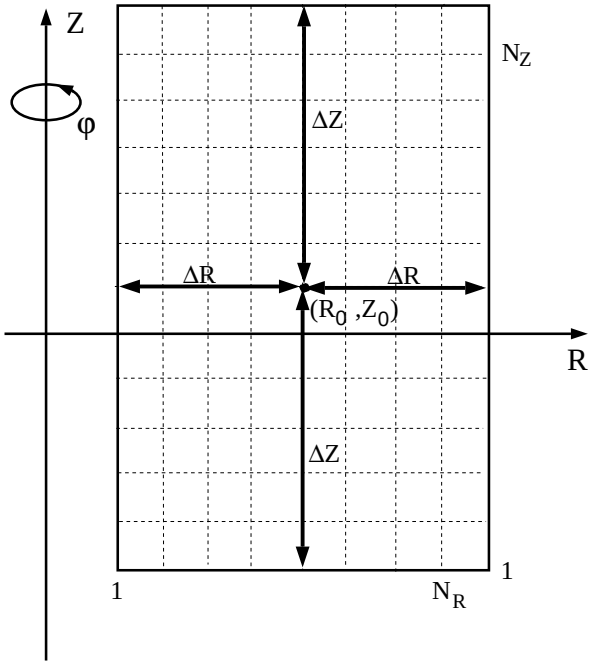

Fig. 3: Toroidal cross-section of the grid box. The magnetic field is computed for N_R grid points in radial direction, N_φ grid points in toroidal direction and N_Z grid points in Z direction.

3.2 CURVILINEAR COORDINATES

MFBE_2001 uses the curvilinear coordinate system (s, v, u) shown in Fig. 4 with s being the normalized toroidal flux ($0 \le s \le 1$, $s = 0$ corresponds to the magnetic axis and $s = 1$ to the plasma boundary), while v (toroidal) and u (poloidal) are angle-like variables ($0 \le v < N_{\rm p},\ 0 \le u < 1$). These coordinates are related with the cylindrical coordinates (R, φ, Z)

$$R = \sum_{\mathrm{m}=0,\mathrm{n}=-\mathrm{n_b}}^{\mathrm{m_b},\mathrm{n_b}} \hat{r}^{\mathrm{c}}_{\mathrm{m,n}}(s)\cos[2\pi(\mathrm{m}u + \mathrm{n}v)] + \hat{r}^{\mathrm{s}}_{\mathrm{m,n}}(s)\sin[2\pi(\mathrm{m}u + \mathrm{n}v)]$$

$$\varphi = \frac{2\pi}{N_{\rm p}} v \tag{12}$$

$$Z = \sum_{\mathrm{m}=0,\mathrm{n}=-\mathrm{n_b}}^{\mathrm{m_b},\mathrm{n_b}} \hat{z}^{\mathrm{c}}_{\mathrm{m,n}}(s)\cos[2\pi(\mathrm{m}u + \mathrm{n}v)] + \hat{z}^{\mathrm{s}}_{\mathrm{m,n}}(s)\sin[2\pi(\mathrm{m}u + \mathrm{n}v)]$$

with $\{\hat{r}^{\mathrm{c}}_{\mathrm{m,n}}(s), \hat{r}^{\mathrm{s}}_{\mathrm{m,n}}(s), \hat{z}^{\mathrm{c}}_{\mathrm{m,n}}(s), \hat{z}^{\mathrm{s}}_{\mathrm{m,n}}(s)\}$ being the Fourier coefficients of a flux surface with normalized toroidal flux s. $\mathrm{N_p}$ is the number of periods, $0 \le \mathrm{m} \le \mathrm{m_b}$ are the poloidal mode numbers and $-\mathrm{n_b} \le \mathrm{n} \le \mathrm{n_b}$ are the toroidal mode numbers.

The corresponding covariant basis vectors are

$$\mathbf{r}_{,s} = \frac{\partial \mathbf{r}}{\partial s} = \frac{\partial R}{\partial s}\hat{\mathbf{e}}_R + \frac{\partial Z}{\partial s}\hat{\mathbf{e}}_Z$$

$$\mathbf{r}_{,v} = \frac{\partial \mathbf{r}}{\partial v} = \frac{\partial R}{\partial v}\hat{\mathbf{e}}_R + R\frac{2\pi}{N_{\rm p}}\hat{\mathbf{e}}_\varphi + \frac{\partial Z}{\partial v}\hat{\mathbf{e}}_Z \tag{13}$$

$$\mathbf{r}_{,u} = \frac{\partial \mathbf{r}}{\partial u} = \frac{\partial R}{\partial u}\hat{\mathbf{e}}_R + \frac{\partial Z}{\partial u}\hat{\mathbf{e}}_Z$$

with

$$\mathbf{r} = R\hat{\mathbf{e}}_R + Z\hat{\mathbf{e}}_Z \tag{14}$$

and the Jacobian

$$\sqrt{g} = \frac{\partial \mathbf{r}}{\partial s} \cdot \frac{\partial \mathbf{r}}{\partial v} \times \frac{\partial \mathbf{r}}{\partial u} = \frac{1}{2}\left(\frac{2\pi}{N_{\rm p}}\right)\left(\frac{\partial R^2}{\partial s}\frac{\partial Z}{\partial u} - \frac{\partial Z}{\partial s}\frac{\partial R^2}{\partial u}\right). \tag{15}$$

$(\hat{\mathbf{e}}_R, \hat{\mathbf{e}}_\varphi, \hat{\mathbf{e}}_Z)$ are the basis vectors of the cylindrical coordinates.

The equilibrium magnetic field in terms of its contravariant components is defined by

$$\mathbf{B}_{\rm p} = B^v\frac{\partial \mathbf{r}}{\partial v} + B^u\frac{\partial \mathbf{r}}{\partial u} \tag{16}$$

with

$$B^v = \sum_{\mathrm{m}=0,\mathrm{n}=-\mathrm{n_b}}^{\mathrm{m_b},\mathrm{n_b}} \hat{b}^{v,\mathrm{c}}_{\mathrm{m,n}}(s)\cos[2\pi(\mathrm{m}u+\mathrm{n}v)] + \hat{b}^{v,\mathrm{s}}_{\mathrm{m,n}}(s)\sin[2\pi(\mathrm{m}u+\mathrm{n}v)]$$

$$B^u = \sum_{\mathrm{m}=0,\mathrm{n}=-\mathrm{n_b}}^{\mathrm{m_b},\mathrm{n_b}} \hat{b}^{u,\mathrm{c}}_{\mathrm{m,n}}(s)\cos[2\pi(\mathrm{m}u+\mathrm{n}v)] + \hat{b}^{u,\mathrm{s}}_{\mathrm{m,n}}(s)\sin[2\pi(\mathrm{m}u+\mathrm{n}v)] \qquad (17)$$

and $\{\hat{b}^{v,\mathrm{c}}_{\mathrm{m,n}}(s), \hat{b}^{v,\mathrm{s}}_{\mathrm{m,n}}(s), \hat{b}^{u,\mathrm{c}}_{\mathrm{m,n}}(s), \hat{b}^{u,\mathrm{s}}_{\mathrm{m,n}}(s)\}$ being the Fourier coefficients of a flux surface with normalized toroidal flux s.

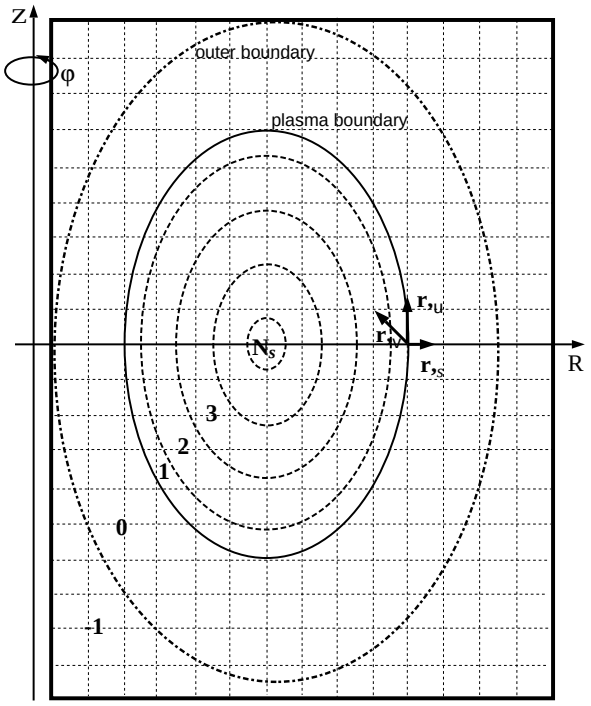

Fig. 4: Flux surfaces (dashed lines) on which the Fourier coefficients of the magnetic field are given, plasma boundary (solid line), outer boundary (dashed-dotted line) and frame of the grid box (thick solid line) for a toroidal cross-section. The arrows represent the curvilinear basis vector $(\mathbf{r}_s, \mathbf{r}_v, \mathbf{r}_u)$, while the numbers are indicies which characterize the positions of the grid points with respect to the surfaces.

The VMEC/NEMEC code yields the Fourier coefficients of a number N_s of discrete flux surfaces and of the magnetic field on surfaces in between (see Section 2.1). Fourier coefficients for arbitrary s values are obtained by a linear interpolation of the coefficients between two neigbouring flux surfaces. As an example the interpolation is given for $\hat{r}^{\mathrm{c}}_{\mathrm{m,n}}(s)$

$$\hat{r}^{\mathrm{c}}_{\mathrm{m,n}}(s) = \hat{r}^{\mathrm{c}}_{\mathrm{m,n}}(s_{\mathrm{i}}) \left(1 - \frac{s-s_{\mathrm{i}}}{\Delta s}\right) + \hat{r}^{\mathrm{c}}_{\mathrm{m,n}}(s_{\mathrm{i+1}}) \left(\frac{s-s_{\mathrm{i}}}{\Delta s}\right) \qquad (18)$$

with $\Delta s = s_{\mathrm{i}+1} - s_{\mathrm{i}}$.

Comparison of the definitions of the curvilinear coordinates Eqs (3) and (4) used in VMEC/NEMEC with the definitions Eqs (12) and (17) used in MFBE_2001 shows that the following transformations of the Fourier coefficients are necessary.

$$\{\hat{r}^{\mathrm{c}}_{\mathrm{m,n}}, \hat{r}^{\mathrm{s}}_{\mathrm{m,n}}, \hat{z}^{\mathrm{c}}_{\mathrm{m,n}}, \hat{z}^{\mathrm{s}}_{\mathrm{m,n}}, \hat{b}^{v,\mathrm{c}}_{\mathrm{m,n}}, \hat{b}^{v,\mathrm{s}}_{\mathrm{m,n}}, \hat{b}^{u,\mathrm{c}}_{\mathrm{m,n}}, \hat{b}^{u,\mathrm{s}}_{\mathrm{m,n}}\}_{\mathrm{MFBE\_2001}}$$

$$= \left\{\hat{r}^{\mathrm{c}}_{\mathrm{m,-n}}, \hat{r}^{\mathrm{s}}_{\mathrm{m,-n}}, \hat{z}^{\mathrm{c}}_{\mathrm{m,-n}}, \hat{z}^{\mathrm{s}}_{\mathrm{m,-n}}, \frac{\mathrm{N_p}}{2\pi}\hat{b}^{\zeta,\mathrm{c}}_{\mathrm{m,-n}}, \frac{\mathrm{N_p}}{2\pi}\hat{b}^{\zeta,\mathrm{s}}_{\mathrm{m,-n}}, \frac{1}{2\pi}\hat{b}^{\theta,\mathrm{c}}_{\mathrm{m,-n}}, \frac{1}{2\pi}\hat{b}^{\theta,\mathrm{s}}_{\mathrm{m,-n}}\right\}_{\mathrm{VMEC/NEMEC}} \tag{19}$$

MFBE_2001 computes the Fourier coefficients of the magnetic field on the plasma boundary and on the magnetic axis by linear extrapolation from the neighbouring inner, respectively, outer surfaces. The Fourier coefficients of the flux surfaces are computed for surfaces lying in between (dashed lines in Fig. 2 and Fig. 4) by linear interpolation (Eq. (18)) in order to get them for the same surfaces on which the Fourier coefficients of the magnetic field are given. The surfaces are counted from the outside to the inside.

Since the grid box has a rectangular toroidal cross-section, it may include grid points that are far away from the plasma boundary where the knowledge of the magnetic field is not needed. Therefore, an outer boundary (dashed-dotted line in Fig. 4) is introduced which is adopted to the geometry of the plasma boundary. The magnetic field on grid points lying outside this boundary is not computed. This selection saves computational time.

For computing the magnetic field on a grid point it is necessary to know whether the point lies outside or inside the plasma boundary. If it lies inside the boundary its curvilinear coordinates have to be calculated. For this purpose, it has to be determined between which surfaces the grid point is located. This is done by using the method of complex integration

$$\oint_{\mathrm{C_p}} \frac{1}{z - z_0} dz = \begin{cases} 0 & z_0 \text{ outside} \\ 2\pi i & z_0 \text{ inside} \end{cases} \tag{20}$$

with $z = R + iZ$ being a complex variable. For a grid point $\mathrm{P}(R_0, \varphi_0, Z_0)$ the closed line $\mathrm{C_p}$ is defined by the cut of flux surface j with the corresponding toroidal plane characterized by the toroidal angle φ_0. Only the imaginary part of the integral Eq.(20) has to be computed. In curvilinear coordinates it is given by

$$\mathrm{Im}I = i \oint_{\mathrm{C_p}} \left(\frac{(R - R_0)}{(R - R_0)^2 + (Z - Z_0)^2} \frac{\partial Z}{\partial u} - \frac{(Z - Z_0)}{(R - R_0)^2 + (Z - Z_0)^2} \frac{\partial R}{\partial u} \right) du \tag{21}$$

with $R = R(s_{\mathrm{j}}, v_0, u)$, $Z = Z(s_{\mathrm{j}}, v_0, u)$ and $v_0 = N_{\mathrm{p}}\varphi_0/2\pi$. If the integral Eq. (21) yields $2\pi i$ for surface j and zero for surface j + 1 then the grid point lies between these two

surfaces. By means of this method each grid point is characterized by an index j (see Fig. 4).

For grid points lying inside the plasma boundary ($\mathrm{j} \geq 1$) the curvilinear coordinates (s_0, v_0, u_0) have to be determined. While v_0 is simply given by the relation $v_0 = N_\mathrm{p}\varphi_0/2\pi$ the coordinates s_0 and u_0 have to be computed by searching a zero of the two nonlinear functions

$$R_0 - \sum_{\mathrm{m}=0,\mathrm{n}=-\mathrm{n_b}}^{\mathrm{m_b},\mathrm{n_b}} \hat{r}^{\mathrm{c}}_{\mathrm{m,n}}(s)\cos[2\pi(\mathrm{m}u + \mathrm{n}v_0)] + \hat{r}^{\mathrm{s}}_{\mathrm{m,n}}(s)\sin[2\pi(\mathrm{m}u + \mathrm{n}v_0)] = 0$$

$$Z_0 - \sum_{\mathrm{m}=0,\mathrm{n}=-\mathrm{n_b}}^{\mathrm{m_b},\mathrm{n_b}} \hat{z}^{\mathrm{c}}_{\mathrm{m,n}}(s)\cos[2\pi(\mathrm{m}u + \mathrm{n}v_0)] + \hat{z}^{\mathrm{s}}_{\mathrm{m,n}}(s)\sin[2\pi(\mathrm{m}u + \mathrm{n}v_0)] = 0. \tag{22}$$

For this purpose, routine C05PBE of the NAG library is used (see Section 4.2). Knowing the curvilinear coordinates of the grid point, the magnetic field is computed using Eq. (16).

For $\mathrm{j} = 0$ the grid point lies inside the outer boundary but outside the plasma boundary. In this case the magnetic field is computed by using the 'virtual casing' principle Eq. (11). With $\mathbf{B}_S = \mathbf{B}_\mathrm{p}(s = 1)$ being the magnetic field on the plasma boundary, its normal vector

$$\mathbf{n} = \frac{\mathbf{N}}{N} = \frac{\frac{\partial \mathbf{r}}{\partial v} \times \frac{\partial \mathbf{r}}{\partial u}}{\left| \frac{\partial \mathbf{r}}{\partial v} \times \frac{\partial \mathbf{r}}{\partial u} \right|}, \tag{23}$$

the surface element

$$df = \left| \frac{\partial \mathbf{r}}{\partial v} \times \frac{\partial \mathbf{r}}{\partial u} \right| dvdu \tag{24}$$

and use of Eq. (9) we obtain for Eq. (11)

$$\mathbf{B_j} = -\frac{\mu_0}{4\pi} \int_S dvdu \frac{(\mathbf{B}'_S(v,u) \times \mathbf{N}'(v,u)) \times (\mathbf{r} - \mathbf{r}'(v,u))}{|\mathbf{r} - \mathbf{r}'(v,u)|^3}. \tag{25}$$

For $\mathrm{j} = -1$ the grid point lies outside the outer boundary and the magnetic field is not computed, but set to zero ($\mathbf{B} = 0$).

3.3 NON-EQUIDISTANT INTEGRATION MESH

In order to obtain a high numerical accuracy, in Eq. (25) the number of integration points has to be adapted to the distance of the grid point from the plasma boundary. Since this distance may be very small for some grid points, a non-equidistant integration mesh is used. To this end, for each grid point P(R_0, φ_0, Z_0) with index j=0 (see Fig. 4) its minimum distance from the plasma surface and its projection (v_S, u_S) onto this surface is determined. Here again the toroidal coordinate v_S is simply given by $v_S = \frac{N_p \varphi_0}{2\pi}$, while the poloidal coordinate u_S is determined by searching the minimum of the following function.

$$f(u) = (R(s=1, v_S, u) - R_0)^2 + (Z(s=1, v_S, u) - Z_0)^2 \tag{26}$$

For this purpose, routine E04BBE of the NAG library is used (see Section 4.2). It returns the minimum $f(u_S)$ and the poloidal coordinate u_S. From this value the minimum distance is computed.

$$\Delta r_{\min} = \sqrt{f(u_S)} \tag{27}$$

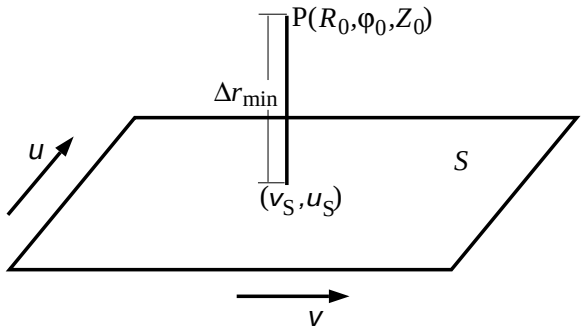

Fig. 5: Projection (v_S, u_S) of the grid point P(R_0, φ_0, Z_0) onto the plasma surface S and its minimum distance $\Delta r_{\min}$ from this surface.

Around the point (v_S, u_S) the integration interval is set to

$$\Delta u_{\min} = \Delta u \frac{\Delta r_{\min}}{c_3 U_{\rm pol}}, \qquad \Delta v_{\min} = \Delta u_{\min} \tag{28}$$

with $\Delta u = 1/\mathrm{N}_u$ being the equidistant integration mesh size in poloidal direction, the average poloidal circumference $U_{\rm pol} = 2\pi a_0$ (a_0=minor radius) and the free parameter c_3 which influences the numerical accuracy. It has to provide that $\Delta v_{\min}$ and $\Delta u_{\min}$ are much smaller than the distance of the grid point from the plasma surface. Further away from this point the integration interval is increased step by step

$$\Delta v_{\rm i} = 2^{({\rm i}-1)c_4} \Delta v_{\min}, \qquad \Delta u_{\rm i} = 2^{({\rm i}-1)c_4} \Delta u_{\min} \tag{29}$$

to an upper limit that corresponds to the equidistant grid size $(\Delta v, \Delta u)$ with $\Delta v = 1/\mathrm{N}_v$ being the equidistant integration mesh size in toroidal direction. In Eq. (29) index i counts

the integration steps, while the free parameter c_4 determines the growth of the integration interval. In Fig. 6 the non-equidistant integration mesh embedded in the equidistant one is shown.

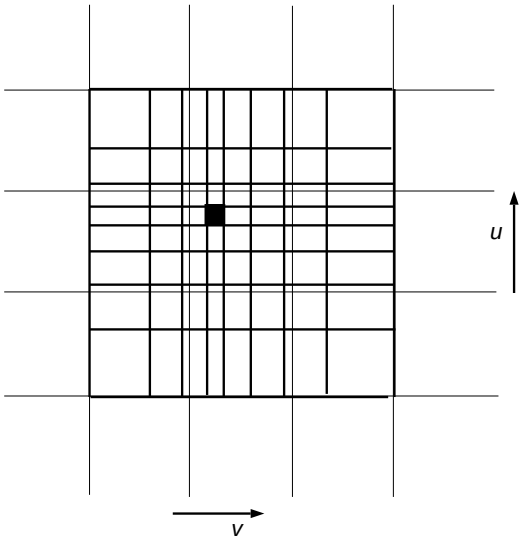

Fig. 6: Draft of the non-equidistant integration mesh embedded in the equidistant one.

The integration over the plasma surface Eq. (25) is splitted into equidistant parts and the non-equidistant part as shown in Fig. 7. Then all parts are summed up.

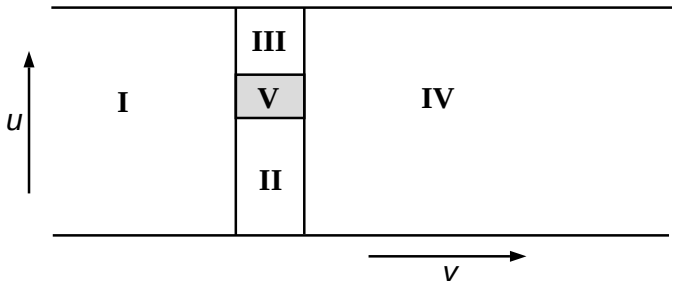

Fig. 7: Equidistant parts (I-IV) and non-equidistant part V of the surface integral.

For grid point distances smaller than a very small fraction of the minor radius a_0

$$\Delta r_{\min} \leq c_2 a_0, \tag{30}$$

the magnetic field is computed on the plasma boundary using Eq. (16). In Eq. (30) c_2 is a free parameter which should be $\leq 1 \cdot 10^{-3}$.

4. USE OF MFBE_2001

MFBE_2001 is written in FORTRAN 90 using free allocation of the field dimensions and free format. Due to the parallelization two code versions are available. One code version uses the native CRAY shmem communication library and runs on a CRAY T3E, while the other uses the MPI communication library and runs on an IBM Regatta supercomputer.

The directory of MFBE_2001 has the following structure:

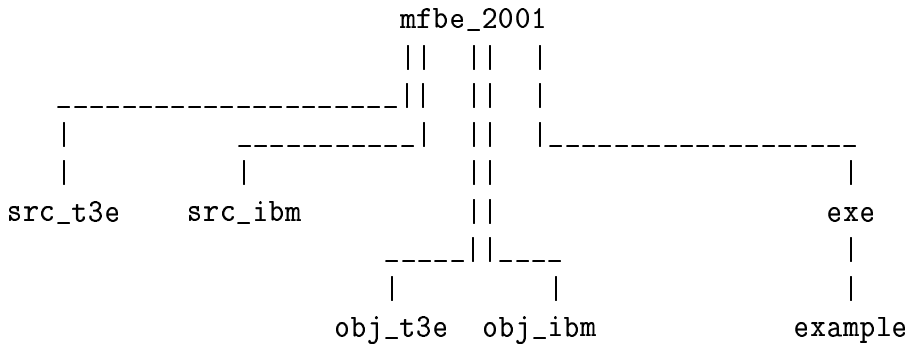

The source code is in subdirectory **src**, while the makefile and the object code are in subdirectory **obj**. Subdirectory **exe** contains the executables and the subdirectory **example**. The suffixes **t3e** and **ibm** mark the code versions.

4.1 SOURCE CODE

MFBE_2001 contains the following modules, includes, main routine and subroutines.

List of modules:

mod_konst.f90	constants and variables used in various subroutines
only src_t3e	
mod_parallel.f90	quantities concerning the parallelization
only src_ibm	
mod_cosinu.f90	fields used for the equidistant integration
mod_field.f90	magnetic field and curvilinear coordinates
mod_four.f90	Fourier coefficients
mod_integ.f90	fields used for the non-equidistant integration
mpp_functions.f90	establishes a MPP job environment

List of includes (only src_t3e):

cosinu.inc	fields used for the equidistant integration
field.inc	magnetic field and curvilinear coordinates
four.inc	Fourier coefficients
integ.inc	fields used for the non-equidistant integration

Main routine:

mfbe.f90	main program

List of subroutines:

axis.f90	computation of R and Z coordinates of the magnetic axis
bfield.f90	determination of the curvilinear coordinates, determination of the minimum distances of grid points from the plasma boundary, computation of the magnetic field
bplasbound.f90	computation of the field on the plasma surface (Eq. (16))
collect.f90	collection of the equidist. parts of the surface integral (Eq. (25))
compint.f90	complex integration (Eq. (21))
curvicoor.f90	computation of the curvilinear coordinates (s, u) (Eq. (22))
equimesh.f90	computation of quantities on the equidistant integration mesh
equint.f90	computation of B_j (Eq. (25)) with the equidist. integration mesh
fcnc05pbe.f90	subroutine for NAG routine C05PBE
fcne04bbe.f90	subroutine for NAG routine E04BBE
fourier.f90	reading, transformation (Eq. (19)) and interpolation (Eq. (18)) of the Fourier coefficients
line.f90	computation of the closed line C_p for the complex integration (Eq. (21))
nonequint.f90	non-equidistant mesh and integration
partint.f90	equidistant integration (Eq. (25)) over parts of the plasma surface
point.f90	computation of R and Z coordinates (Eq. (12))

List of external functions (only src_t3e):

npid.f90	yields the processor number
nprocs.f90	yields the total number of processors

4.2 LIBRARY ROUTINES

MFBE_2001 uses the NAG library routines C05PBE and E04BBE. Note, these routines are named C05PBF and E04BBF in the IBM version of the code.

C05PBE

C05PBE is a routine to find a zero of a system of N nonlinear functions in N variables. Here it is used to determine the curvilinear coordinates s_0 and u_0 for given cylindrical coordinates R_0 and Z_0 (Eq. (22)). The NAG routine needs subroutine fcnc05pbe.f90.

E04BBE

In a given finite interval E04BBE searches for a minimum of a continuous function of a single variable, using function and first derivative values. The method is intended for functions which have a continous first derivative. Here, the NAG routine is used to search the minimum of function Eq. (26). It needs subroutine fcne04bbe.f90.

4.3 MAKEFILE

In the subdiretories **obj_t3e** and **obj_ibm** are the makefiles for the two code versions. They create the executables MFBE_2001_T3E and MFBE_2001_IBM in subdirectory **exe**.

4.4 INPUT

MFBE_2001 uses MKS-units, that is, all input and output quantities are given in these units. The code needs three input files.

INPUT 1: standard input

INPUT 1 contains names of non-standard input and output files as well as parameters concerning the work of the code. The input quantities are read in program mfbe.f90 and subroutine fourier.f90.

Example of a standard input file

```
in_equilibrium: '/u/ers/mhd/mfbe_2001/exe/example_t3e/wout.12224'
format_type:    'ascii'
in_field:       '/u/ers/mhd/mfbe_2001/exe/example_t3e/field_vac_12224'
format_type:    'ascii'
out_field:      '/u/ers/mhd/mfbe_2001/exe/example_t3e/field_mfbe_12224'
format_type:    'ascii'
configuration:  'ASDEX Upgrade'
                 r0m    a0m
                 1.65   0.5
stop:           'out_boundary'
test:           'no'
                 nrt1  nrt2  nzt1  nzt2  npht1  npht2
                  1     100   70    70     1      1
complex integration
                 jubmin   icompd   epscom
                  2000       6      1.e-3
determination of the curvilinear coordinates
                 xtol_c05pbe  ifail_c05pbe  seps   dus   nus  icout
                    1.e-5          1       1.e-5   0.05  10    20
determination of the minimum distance
               e1_e04bbe e2_e04bbe db_e04bbe maxcall_e04bbe ifail_e04bbe
                1.e-8      1.e-8     0.30       20             1
equidistant grid for surface integration
                 jud  jvd
                 320  960
non-equidistant grid for surface integration
                 nc1u   nc1v   r2x    r3x   r4x
                  45     45   1.e-3   1.5  0.15
maximum difference between Bc and B
                 dbphimax  dbrmax  dbzmax
                   0.060    0.5     0.75
outer boundary
               msr nsr mnsr
                2   1   2
                m   n     crc          crs          czs          czc
                0   0  1.6250E+00  0.0000E+00   0.0000E+00   0.0000E+00
                1   0  2.5000E+00  0.0000E+00  -2.5000E+00   0.0000E+00
```

List of variables:

Non-standard input and output file names

in_equilibrium	character*80	name of the input file containing the equilibrium quantities (INPUT 3)
format_type	character*80	type of the file format
	binary	
	ascii	
in_field	character*80	name of the input file containing the vacuum field produced by external coils (INPUT 2)
format_type	character*80	type of the file format
	binary	
	ascii	
out_field	character*80	name of the output file containing the computed magnetic field (OUTPUT 2)
format_type	character*80	type of the file format
	binary	
	ascii	

Experiment

configuration	character*80	name of the experiment, e.g. ASDEX Upgrade
r0m	real	major plasma radius
a0m	real	minor plasma radius

Mode

stop	character*80	program stops after:
	read_input	reading of the input data
	curvi_coor	computation of the curvilinear coordinates
	in_boundary	computation of the magnetic field inside the plasma boundary
	min_distance	computation of the minimum distances of grid points from the plasma boundary
	out_boundary	computation of the magnetic field outside the plasma boundary
test	character*80	kind of use of the code
	no	no test
	equilibrium	test of the equilibrium field (Eq.(11))
	vacuum	test of the external vacuum field (Eq.(10))

nrt1	integer	lower grid point in R direction
nrt2	integer	upper grid point in R direction
nzt1	integer	lower grid point in Z direction
nzt2	integer	upper grid point in Z direction
npht1	integer	lower grid point in φ direction
npht2	integer	upper grid point in φ direction

Note, if the code is used in the test mode (test = *equilibrium* or *vacuum*), then the computation of the magnetic field is limited to grid points lying in the boundaries defined by nrt1, nrt2, nzt1, nzt2, npht1 and npht2. Otherwise, the magnetic field is computed for the complete grid defined in INPUT 2.

Complex integration (Eq.(21))

jubmin	integer	minimum number of integration points
icompd	integer	jubmin $\cdot\, 2^{\text{icompd}}$ = maximum number of integration points
epscom	real	accuracy of the integration

Determination of the curvilinear coordinates (s, u) (Eq. (22))

xtol_c05pbe	real	specifies the accuracy to which the solution of C05PBE is required. The recommended value is the square root of the machine precision.
ifail_c05pbe	integer	must be set to 0, -1, or 1
seps	real	accuracy of the s coordinate
dus	real	step size for the search of the u coordinate
nus	integer	number of initial u values
icout	integer	total number of attemps to determine s and u

Determination of the minimum distance (Eq. (27))

e1_e04bbe	real	relative accuracy to which the position of the minimum is required
e2_e04bbe	real	absolute accuracy to which the position of the minimum is required
db_e04bbe	real	2·db_e04bbe = width of the interval in which the minimum is searched
maxcall_e04bbe	integer	maximum number of calls of fcne04bbe.f90
ifail_e04bbe	integer	must be set to 0 or 1

Equidistant grid for the surface integration (Eq. (25))

jud	integer	number of integration points in poloidal direction
jvd	integer	number of integration points per period in toroidal direction

Non-equidistant grid for the surface integration (Eq. (25))

nc1u	integer	$2 \cdot$ nc1u = number of equidistant grid points in poloidal direction substituted by the non-equidistant grid
nc1v	integer	$2 \cdot$ nc1v = number of equidistant grid points in toroidal direction substituted by the non-equidistant grid
r2x	real	defines the min. distance (c_2 in Eq. (30)) for which $\mathbf{B}_j$ is computed by integration (Eq. (25))
r3x	real	determines the minimum cell size of the non-equidistant grid (c_3 in Eq. (28))
r4x	real	determines the increase of the cell size of the non-equidistant grid (c_4 in Eq. (29))

Expected maximum difference between $\mathbf{B}_\mathrm{c}$ *and* $\mathbf{B}$

dbphimax	real	maximum value of $\lvert B_\varphi - B_{\mathrm{c},\varphi}\rvert$
dbrmax	real	maximum value of $\lvert B_R - B_{\mathrm{c},R}\rvert$
dbzmax	real	maximum value of $\lvert B_Z - B_{\mathrm{c},Z}\rvert$

Outer boundary (compare Fig.4)

msr	integer	max. pol. mode number: $0 \leq \mathrm{m} \leq \mathrm{msr} - 1$
nsr	integer	max. tor. mode number: $-\mathrm{nsr} \leq \mathrm{n} \leq \mathrm{nsr}$
mnsr	integer	number of coefficients to be read
m	integer	poloidal mode number
n	integer	toroidal mode number
crc(m,n,0)	real	$\hat{r}^{\mathrm{c}}_{\mathrm{m,n}}$
crs(m,n,0)	real	$\hat{r}^{\mathrm{s}}_{\mathrm{m,n}}$
czs(m,n,0)	real	$\hat{z}^{\mathrm{s}}_{\mathrm{m,n}}$
czc(m,n,0)	real	$\hat{z}^{\mathrm{c}}_{\mathrm{m,n}}$

INPUT 2: external magnetic field

INPUT 2 is the output of the VACFIELD code. It is either an ascii file or a binary file with double precision data of the external magnetic field $\mathbf{B}_c$. This input is read in program mfbe.f90 and subroutine bfield.f90.

List of variables:

Dimensions of the vacuum field

enf	real	number of toroidal plans per period
	enf = 1	axisymmetric field
enr	real	number of grid points in R direction
enz	real	number of grid points in Z direction
ena	real	number of components of the magnetic field
enp	real	number of periods
enfd	real	number of toroidal plans for which the magnetic field is computed
	enfd = nint(enf)/2 + 1	stellarator-symmetric field
	enfd = enf	asymmetric field

Note, in order to avoid difficulties with different integer lengths on different computers, these quantities are defined as real variables in read and write instructions. They are transformed into integer variables inside the code.

Boundaries of the grid (compare Fig. 3)

r00	real	R coordinate of the centre of the box
z00	real	Z coordinate of the centre of the box
dr0	real	half width of the box in R direction
dz0	real	half width of the box in Z direction

Vacuum magnetic field produced by external coils

bb(1,k,l)	real	B_φ component
bb(2,k,l)	real	B_R component
bb(3,k,l)	real	B_Z component

with $1 \leq$ k $\leq$ nr (R direction) and $1 \leq$ l $\leq$ nz (Z direction). For more details see read statements in subroutine bfield.f90.

INPUT 3: equilibrium input

INPUT 3 is an output of the VMEC/NEMEC code. It is either an ascii file or a binary file with double precision data of equilbrium quantities. This input is read in program mfbe.f90 and subroutine fourier.f90.

List of variables:

Dimensions of the fields

gamma	real	adiabatic constant (not needed in MFBE_2001)
enfp	real	number of periods (has to agree with np)
ens	real	number of flux surfaces $1 \leq \mathrm{i} \leq \mathrm{ens}$
empol	real	poloidal mode number $0 \leq \mathrm{m} \leq \mathrm{empol} - 1$
enmax	real	toroidal mode number $-\mathrm{enmax} \leq \mathrm{n} \leq \mathrm{enmax}$
emnmax	real	total mode number
eiasym	real	symmetry
	eiasym = 0	stellarator-symmetric equilibrium
	eiasym = 1	asymmetric equilibrium

Note, inside the code these variables are transformed into integer variables.

Fourier coefficients defining the flux surfaces and the equilibrium magnetic field

crc(m,n,i)	real	$\hat{r}^{\mathrm{c}}_{\mathrm{m},-\mathrm{n}}(s_{\mathrm{i}})$
czs(m,n,i)	real	$\hat{z}^{\mathrm{s}}_{\mathrm{m},-\mathrm{n}}(s_{\mathrm{i}})$
crs(m,n,i)	real	$\hat{r}^{\mathrm{s}}_{\mathrm{m},-\mathrm{n}}(s_{\mathrm{i}})$
czc(m,n,i)	real	$\hat{z}^{\mathrm{c}}_{\mathrm{m},-\mathrm{n}}(s_{\mathrm{i}})$
bsuc(m,n,j)	real	$\hat{b}^{\theta,\mathrm{c}}_{\mathrm{m},-\mathrm{n}}(s_{\mathrm{j}})$
bsvc(m,n,j)	real	$\hat{b}^{\zeta,\mathrm{c}}_{\mathrm{m},-\mathrm{n}}(s_{\mathrm{j}})$
bsus(m,n,j)	real	$\hat{b}^{\theta,s}_{\mathrm{m},-\mathrm{n}}(s_{\mathrm{j}})$
bsvs(m,n,j)	real	$\hat{b}^{\zeta,s}_{\mathrm{m},-\mathrm{n}}(s_{\mathrm{j}})$

For more details see read statements in subroutine fourier.f90.

4.5 HOW TO RUN THE CODE

MFBE_2001 is a parallelized code. It computes the magnetic field on a two-dimensional (axisymmetric) or a three-dimensional grid. If the configuration exhibits axisymmetry, the magnetic field only has to be computed for one toroidal cross-section. Then the

computation is parallelized in Z direction. For the three-dimensional problem the code is parallelized in toroidal direction. It has to be made sure that either the number of grid points in Z direction (two-dimensional case) or the number of grid points in toroidal direction (three-dimensional case) is a multiple of the number of used processors. For a good performance of the code the number of processors should be a power of two.

The subdirectory **example** contains example files for an axisymmetric configuration. There the input, output and script files are given for interactive tests and batch jobs.

test

input_test	INPUT 1: standard input
field_vac_12224	INPUT 2: magnetic field of external coils
wout.12224	INPUT 3: equilibrium input
mfbe_t3e.e	script for an interactive run on a CRAY T3E
mfbe_ibm.e	script for an interactive run on an IBM Regatta
output_test	OUTPUT 1: standard output

batch job

input	INPUT 1: standard input
field_vac_12224	INPUT 2: magnetic field of external coils
wout.12224	INPUT 3: equilibrium input
mfbe_t3e.j	script for a batch job on a CRAY T3E
mfbe_ibm.j	script for a batch job on an IBM Regatta
output	OUTPUT 1: standard output
field_mfbe_12224	OUTPUT 2: computed magnetic field

The results of this example are discussed in detail in Chapter 5.1.

4.6 OUTPUT

The code produces two output files. All output quantities are given in MKS units.

OUTPUT 1: standard output

OUTPUT 1 contains all informations of INPUT 1 and possible warnings and error messages of the code.

WARNINGS

```
WARNING 1: magnetic field of grid point (i,ir,iz) could not be calculated
```

(i,ir,iz) are the indices of the grid point in toroidal, radial and Z direction.

If for a grid point the difference between the computed field $\mathbf{B}$ and the external field $\mathbf{B}_c$ is larger than the expected maximum difference given in INPUT 1, then WARNING 2 occurs.

```
WARNING 2: (i,ir,iz) ibes(ir,iz) db1 db2 db3
```

Again, (i,ir,iz) are the indices of the grid point in toroidal, radial and Z direction, while ibes(ir,iz) is the index which characterizes the position of the grid point with respect to the nested flux surfaces (see Fig. 4). db1, db2 and db3 are the absolut amounts of the differences between the components of the two fields in toroidal, radial and Z direction. If these amounts are unrealisticly high, an error has occured during the computation of the magnetic field of this grid point.

If the NAG routine E04BBE returns with ifail$\neq$0, WARNING 3 is written.

```
WARNING 3: (i,ir,iz) ifail umin fmin
```

Here ifail is the index of the error message of E04BBE (for details see NAG manual), while umin and fmin correspond to u_0 and $f(u_0)$ of Eq.(27) which have been computed by E04BBE.

ERRORS

The program stops with an error message if an input or output file could not be opened. It also stops computation if one of the following errors occurs.

```
PARALLELIZATION: toroidal direction
ERROR: ***** npes = ????? *****
```

This error message occurs if the number of toroidal planes for which the magnetic field has to be computed is not a multiple of the number of used processors (three-dimensional case).

```
PARALLELIZATION: Z direction
ERROR: ***** npes = ????? *****
```

This error message occurs if the number of grid points in Z direction is not a multiple of the number of used processors (axisymmetric case).

If the code is used in the test mode additional information is written in the standard output file.

Test mode 'equilibrium'

```
equilibrium: 1 73 65 43 -2.0177 -0.0640 -0.3164 ss0  =0.8863 uu0=0.9619
vacuum     : 1 73 65 43 -2.0167  0.0041 -0.1485
equilibrium: 1 74 65 36 -2.0001 -0.0611 -0.3171 ss0  =0.9511 uu0=0.9640
vacuum     : 1 74 65 36 -1.9993  0.0038 -0.1492
equilibrium: 1 75 65 28 -1.9827 -0.0581 -0.3165 ss0  =0.8426 uu0=0.9660
vacuum     : 1 75 65 28 -1.9822  0.0036 -0.1500
equilibrium: 1 76 65 19 -1.9656 -0.0553 -0.3151 ss0  =0.6681 uu0=0.9679
vacuum     : 1 76 65 19 -1.9654  0.0033 -0.1507
equilibrium: 1 77 65  9 -1.9490 -0.0522 -0.3111 ss0  =0.6857 uu0=0.9697
vacuum     : 1 77 65  9 -1.9488  0.0030 -0.1515
vacuum     : 1 78 65  0 -1.9326  0.0027 -0.1522
equi. korr.: 1 78 65  0 -0.0017  0.0519  0.1535 dabst=0.0053 uus=0.9711
equi. vac. : 1 78 65  0 -1.9309 -0.0492 -0.3057
vacuum     : 1 79 65  0 -1.9166  0.0024 -0.1529
equi. korr.: 1 79 65  0 -0.0014  0.0488  0.1474 dabst=0.0226 uus=0.9717
equi. vac. : 1 79 65  0 -1.9152 -0.0464 -0.3003
vacuum     : 1 80 65  0 -1.9009  0.0021 -0.1536
equi. korr.: 1 80 65  0 -0.0012  0.0459  0.1417 dabst=0.0399 uus=0.9723
equi. vac. : 1 80 65  0 -1.8997 -0.0438 -0.2953
```

There, the first three columns of integers are the indices of the grid point in toroidal, radial and Z direction, while the forth column contains the index j which characterizes the position of the grid point with respect to the nested flux surfaces. The three columns of real numbers are the three components (toroidal, radial and Z direction) of one of the following fields:

equilibrium:	equilibrium magnetic field $\mathbf{B}_\mathrm{p}$ (Eq. (16))
vacuum:	magnetic field of external coils $\mathbf{B}_\mathrm{c}$ (INPUT 2)
equi. korr.:	magnetic field created by the surface current $\mathbf{j}_S$, but oppsite in sign, that is, $-\mathbf{B}_\mathrm{j}$ (Eq. (11))
equi. vac. :	vacuum magnetic field of the equilibrium ($\mathbf{B}$ in Eq. (8))

ss0 and **uu0** are the curvilinear coordinates(s, u) of the grid point, while **dabst** is its minimum distance (Eq. (27)) from the plasma boundary. The projection of the grid point onto the plasma surface is given by **uus** (poloidal coordinate).

Test mode 'vacuum'

```
vacuum     : 1 73 65 43 -2.0167  0.0041 -0.1485
equi. korr.: 1 73 65 43 -2.0161  0.0041 -0.1486 dabst=0.0810 uus=0.9677
equi. vac. : 1 73 65 43 -0.0006 -0.0000  0.0001
vacuum     : 1 74 65 36 -1.9993  0.0038 -0.1492
equi. korr.: 1 74 65 36 -1.9985  0.0039 -0.1493 dabst=0.0637 uus=0.9685
equi. vac. : 1 74 65 36 -0.0008 -0.0001  0.000
vacuum     : 1 75 65 28 -1.9822  0.0036 -0.1500
equi. korr.: 1 75 65 28 -1.9812  0.0036 -0.1500 dabst=0.0465 uus=0.9692
equi. vac. : 1 75 65 28 -0.0010 -0.0001  0.0000
vacuum     : 1 76 65 19 -1.9654  0.0033 -0.1507
equi. korr.: 1 76 65 19 -1.9641  0.0034 -0.1507 dabst=0.0292 uus=0.9698
equi. vac. : 1 76 65 19 -0.0012 -0.0001  0.0000
vacuum     : 1 77 65  9 -1.9488  0.0030 -0.1515
equi. korr.: 1 77 65  9 -1.9473  0.0031 -0.1514 dabst=0.0120 uus=0.9705
equi. vac. : 1 77 65  9 -0.0015 -0.0001 -0.0000
vacuum     : 1 78 65  0 -1.9326  0.0027 -0.1522
equi. korr.: 1 78 65  0 -0.0017  0.0519  0.1535 dabst=0.0053 uus=0.9711
equi. vac. : 1 78 65  0 -1.9309 -0.0492 -0.3057
vacuum     : 1 79 65  0 -1.9166  0.0024 -0.1529
equi. korr.: 1 79 65  0 -0.0014  0.0488  0.1474 dabst=0.0226 uus=0.9717
equi. vac. : 1 79 65  0 -1.9152 -0.0464 -0.3003
vacuum     : 1 80 65  0 -1.9009  0.0021 -0.1536
equi. korr.: 1 80 65  0 -0.0012  0.0459  0.1417 dabst=0.0399 uus=0.9723
equi. vac. : 1 80 65  0 -1.8997 -0.0438 -0.2953
```

This output is similar to the output of the test mode 'equilibrium'. Only the definitions of the magnetic field values of the lines 'equi. korr' and 'equi. vac.' are different for grid points lying inside the plasma boundary ($j \geq 1$):

equi. korr.: external magnetic field $\mathbf{B}_c$ inside the plasma boundary (Eq. (10))
equi. vac. : differences between the components of $\mathbf{B}_c$ (INPUT 2) and $\mathbf{B}_c$ (Eq. (10))

OUTPUT 2: computed magnetic field

The possible formats and the data structure of OUTPUT2 are the same as of INPUT2 (see Chapter 4.4).

5. EXAMPLES

Use and possible tests of the accuracy of VMEC/NEMEC+MFBE_2001+GOURDON are discussed for a limiter-defined axisymmetric tokamak equilibrium (Sec. 5.1), a five-periodic stellarator equilibrium without net toroidal current (Sec. 5.2) and a two-periodic quasi-axisymmetric stellarator equilibrium (Sec. 5.3).

5.1 TOKAMAK

For axisymmetric configurations it is possible to compare VMEC/NEMEC+MFBE_2001 results with computations made with the axisymmetric equilibrium DIVA code [13]. The two-dimensional free-boundary DIVA code computes limiter or separatrix-defined plasma equilibria in the magnetic field of an external conductor system by solving the Grad-Shafranov equation. As example a limiter-defined, not up-down symmetric equilibrium of ASDEX Upgrade type (see Fig. 8) is considered with major radius $R_0 = 1.65$ m, inverse aspect ratio $\epsilon = 0.333$, beta poloidal $\beta_{\rm pol} = 0.644\%$ and total toroidal current $I = 0.786$ MA.

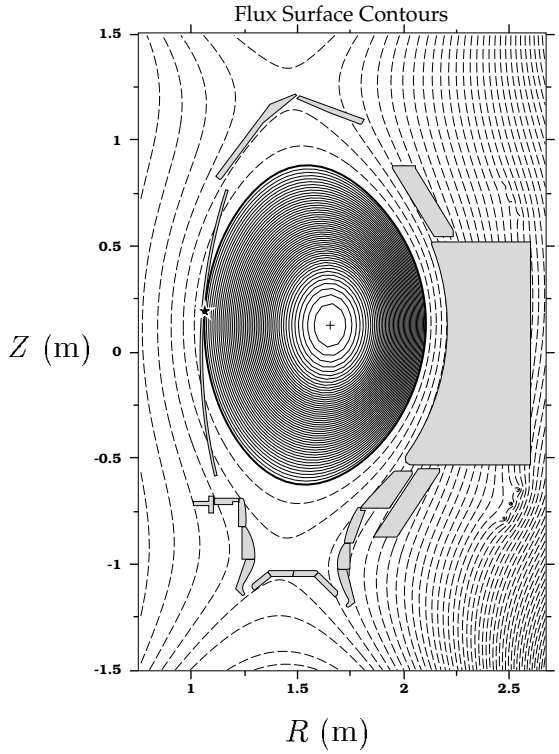

Fig. 8: Flux surfaces of the axisymmetric limiter-defined equilibrium computed with DIVA. The solid black line indicates the plasma boundary, while the grey structures represent the divertor and limiter components. The star marks the position where the plasma intersects a limiter plate.

Recalculating the DIVA equilibrium with the fixed-boundary VMEC code as described in Ref. [14], computing the magnetic field with MFBE_2001 and tracing field lines with GOURDON the Poincaré plot shown in Fig. 9 is obtained. There, the surfaces of the magnetic field are compared with surfaces of constant poloidal flux computed with DIVA.

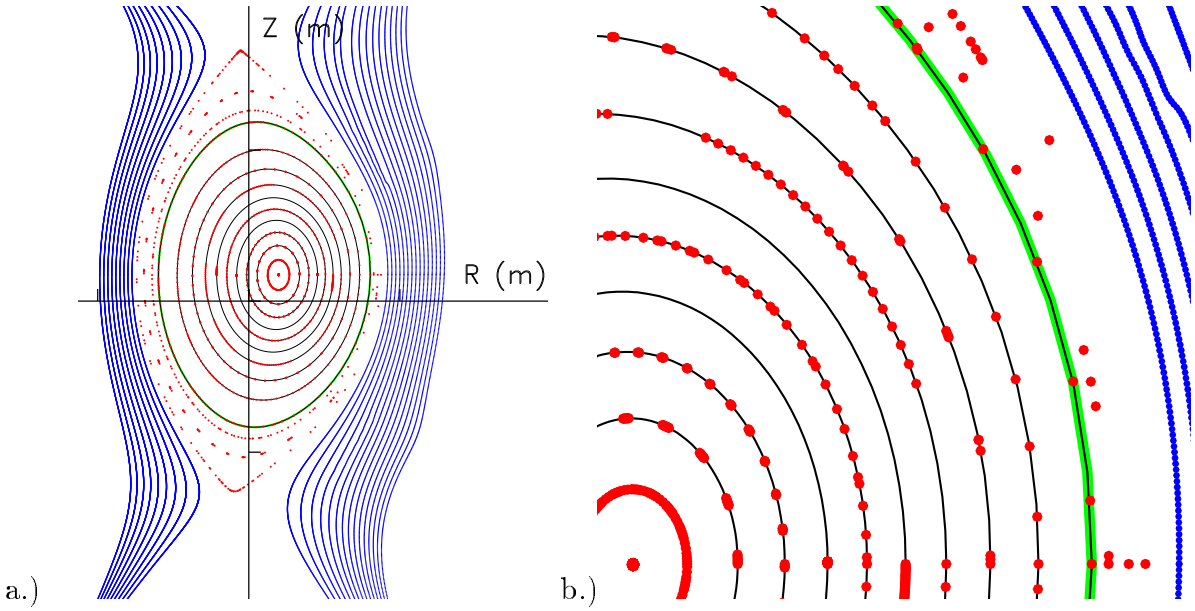

Fig. 9: a.) Poincaré plot of the axisymmetric magnetic field computed with VMEC+ MFBE_2001+GOURDON (red and blue dots) and surfaces of constant poloidal flux calculated with DIVA (green and black lines). The green line indicates the limiter-defined plasma boundary. **b.)** Zoom of the upper right part.

Up to the plasma boundary the surfaces coincide very well. But also in the vacuum region the magnetic field topology agrees with the DIVA solution (compare Fig. 8). There, the closed magnetic surfaces up to the separatrix and the topology of the open field lines could be reproduced.

Using Biot-Savart's law, the VACFIELD code yields the magnetic field of the external conductors. Inside the plasma boundary it is also possible to compute $\mathbf{B}_\mathrm{c}$ by using the 'virtual casing' principle (Eq.(10)). Fig. 10 shows the normalized differences of the external fields $(\mathbf{B}_\mathrm{c}^{\mathrm{VACFIELD}} - \mathbf{B}_\mathrm{c}^{\mathrm{MFBE}})/|B_0|$ with $|B_0| = 2.456$ T being the amount of the external toroidal magnetic field at the radial coordinate $R = 1.65$ m. The components B_φ, B_R and B_Z are plotted as functions of the radial coordinate while the Z coordinate is kept constant. As example a Z coordinate close to the magnetic axis is chosen. The plots demonstrate the high accuracy of the VMEC+MFBE results obtained for this axisymmetric equilibrium. The differences of the fields are negligible.

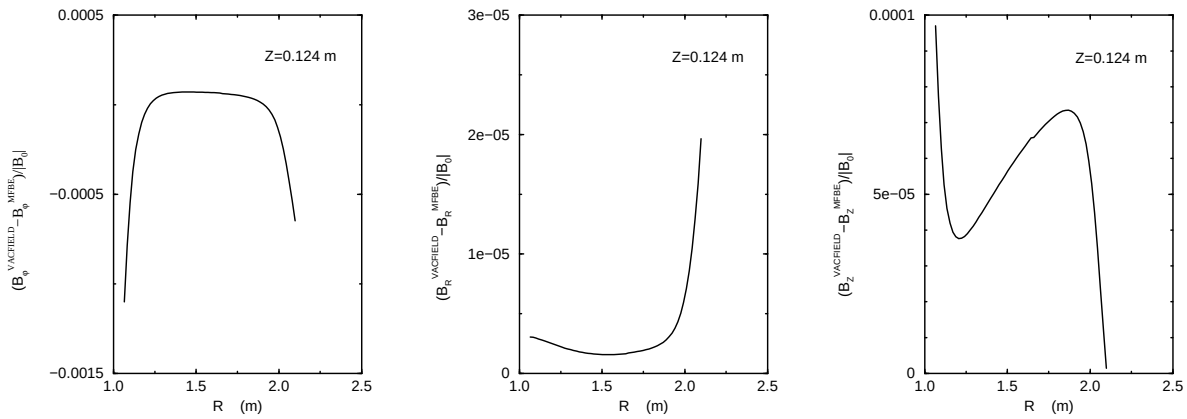

Fig. 10: For a constant Z coordinate the components B_φ, B_R and and B_Z of the normalized differences of the external fields are plotted as functions of the radial coordinate R. The selected Z coordinate is close to the magnetic axis of the equilibrium.

5.2 STELLARATOR WITHOUT NET TOROIDAL CURRENT

For a stellarator without net toroidal current the vacuum magnetic field produced by the external conductor system already exhibits closed magnetic flux surfaces. Comparing such a field computed with the VACFIELD code with the NEMEC+MFBE_2001 solution obtained for the corresponding equilibrium with volume-averaged plasma beta $\langle\beta\rangle = 0$ provides an excellent test of the numerical accuracy of the NEMEC+MFBE_2001 results Ref. [1].

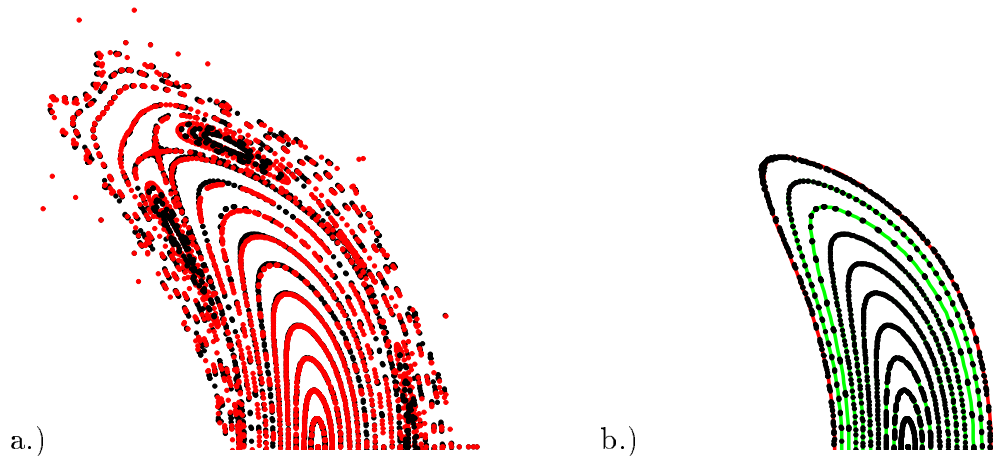

Fig. 11: Upper halves of Poincaré plots of a five-periodic W7-X configuration with $\langle\beta\rangle = 0$. At a symmetric bean-shaped cross-section the topology of the MFBE_2001 magnetic field (black dots) is compared **a.)** with the vacuum field produced by external coils (red dots) and **b.)** with flux surfaces of the NEMEC equilibrium (green solid lines). In **b.)** the red solid line marks the plasma boundary of the equilibrium.

Considering a five-periodic Wendelstein 7-X configuration with major radius $R_0 = 5.5$ m, aspect ratio $A = 10$ and a magnetic field strength of $B_a = 3$ T on the magnetic axis, the magnetic field structure of the MFBE_2001 solution is compared with the topology of the vacuum field (Fig. 11a) and with flux surfaces of the NEMEC equilibrium (Fig. 11b). The MFBE_2001 solution agrees very well with the vacuum field produced by external coils and the NEMEC equilibrium ($\langle\beta\rangle = 0$).

In Fig. 12 the rotational transform profiles obtained from the vacuum field, the NEMEC equilibrium, and the MFBE_2001 magnetic field are plotted. NEMEC only yields values of the rotaional transform up to the plasma boundary. The plateaux at $\iota = 1.0$ and $\iota = 1.1$ correspond to the macroscopic 5/5 and 11/10 islands (see Fig. 11a). The rotational transform profiles agree excellently. Only close to the separatrix of the 5/5 islands the rotational transform obtained from the MFBE magnetic field slightly deviates from the vacuum field value, because X-Points are most sensitive to numerical inaccuracies.

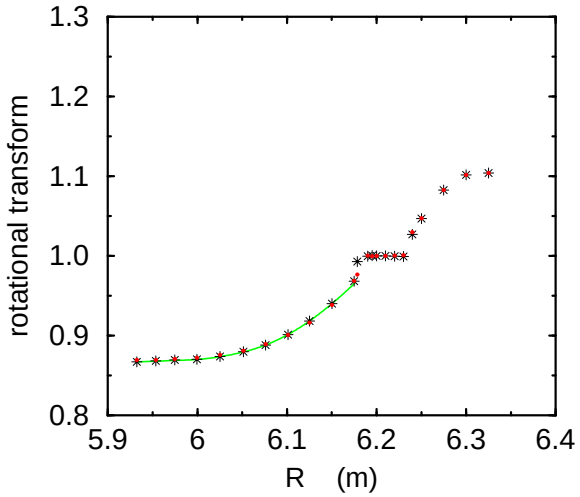

Fig. 12: Rotational transform of the vacuum field (red dots), the NEMEC solution (green solid line) and the MFBE_2001 magnetic field (black stars) as function of the radial coordinate R at the midplane of the beand-shaped cross-section in outward direction.

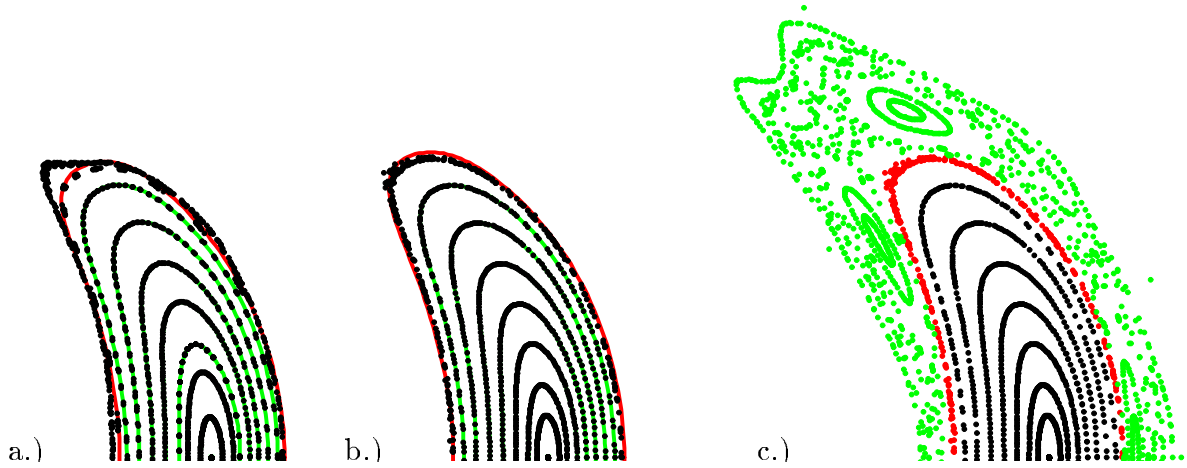

Fig. 13: Upper halves of Poincaré plots of the five-periodic W7-X configuration with $\langle\beta\rangle = 2.5\%$. At a symmetric bean-shaped cross-section flux surfaces of NEMEC equilibria (green solid lines) with **a.)** $\Phi_{\text{total}} = 1.854$ Wb and **b.)** $\Phi_{\text{total}} = 2.004$ Wb are compared with the corresponding MFBE_2001 magnetic field structures (black dots). In **c.)** the full magnetic field structure of the equilibrium with $\Phi_{\text{total}} = 2.004$ Wb is shown. There, closed flux surfaces (black dots) inside the last closed magnetic surface (red dots) and field lines of the edge region (green dots) are plotted.

Figure 13 shows an example of iterative determination of the LCMS. Free-boundary equilibria with various values of total toroidal flux Φ_{total} are computed for the same stellarator configuration as described above, but with $\langle\beta\rangle = 2.5\%$. Their last closed magnetic surfaces are determined and compared with the correponding plasma boundaries. In Fig. 13a the plasma boundary (red line) and its corresponding LCMS (outermost surface, black dots) are plotted for a too small toroidal flux ($\Phi_{\text{total}} = 1.854$ Wb). Then the toroidal flux is increased step by step until the LCMS approximately agrees with the plasma boundary. This is the case for $\Phi_{\text{total}} = 2.004$ Wb as shown in Fig. 13b. In Fig. 13c the full magnetic field structure of the equilibrium with $\Phi_{\text{total}} = 2.004$ Wb is plotted. A comparison of this plot with the vacuum magnetic field structure given in Fig. 11a shows the following properties of the considered optimized Helias configuration. With increasing β the X and O-points of the macroscopic islands approximately keep their positions, while the width of the macroscopic islands increases and the edge region ergodizes.

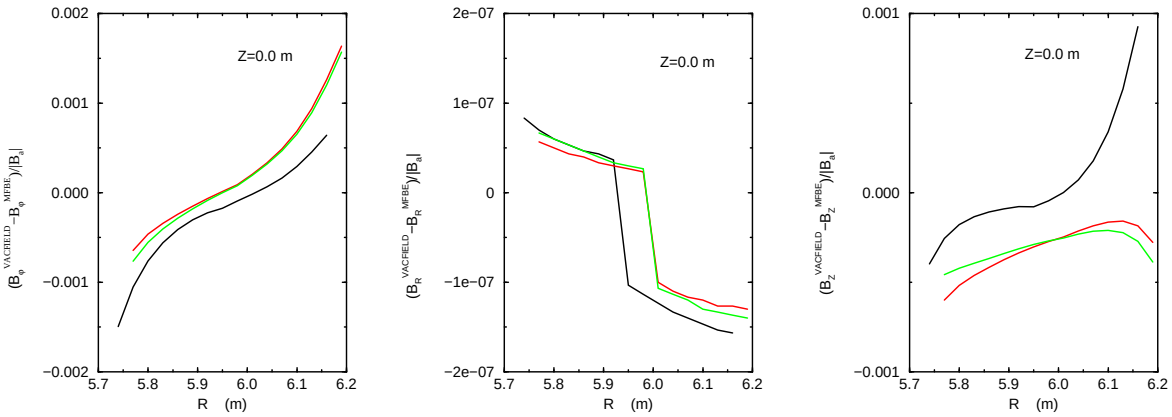

Fig. 14: At the midplane ($Z = 0$) of a bean-shaped cross-section ($\varphi = 0$) the normalized differences of the external fields as functions of the radial coordinate R are plotted for the components B_φ, B_R and B_Z. The black line marks the vacuum case, while the coloured lines represent the two equilibria (red: $\Phi_{\text{total}} = 1.854$ Wb, green: $\Phi_{\text{total}} = 2.004$ Wb).

In Fig. 14 the normalized differences of the magnetic fields $(\mathbf{B}_{\text{c}}^{\text{VACFIELD}} - \mathbf{B}_{\text{c}}^{\text{MFBE}})/|B_{\text{a}}|$ are plotted for the vacuum case and the two finite-β cases shown in Fig. 13a and 13b. Here, the differences are normalized to the magnetic field strength of the vacuum field at the magnetic axis $|B_{\text{a}}| = 3\ T$. At the midplane of the symmetric bean-shaped cross-section the components B_φ, B_R and B_Z are plotted as functions of the radial coordinate. For these cases the differences of the fields are sufficiently small and of comparable size ($\approx 1 \cdot 10^{-3}$). Because of the stellarator symmetry the radial component of the magnetic field B_R has to be zero for the considered φ and Z coordinates. As shown in Fig. 14 the MFBE_2001 field fulfills this symmetry very well.

5.3 QUASI-AXISYMMETRIC STELLARATOR

Quasi-axisymmetric stellarators are three-dimensional configurations which need a net toroidal current in order to produce closed flux surfaces. Figure 15 shows the results obtained for a two-periodic quasi-axisymmetric configuration with major radius $R_0 = 3.5$ m, aspect ratio $A = 0.455$, total toroidal current $I = -0.287$ MA and volume-averaged beta $\langle\beta\rangle = 2.88\%$.

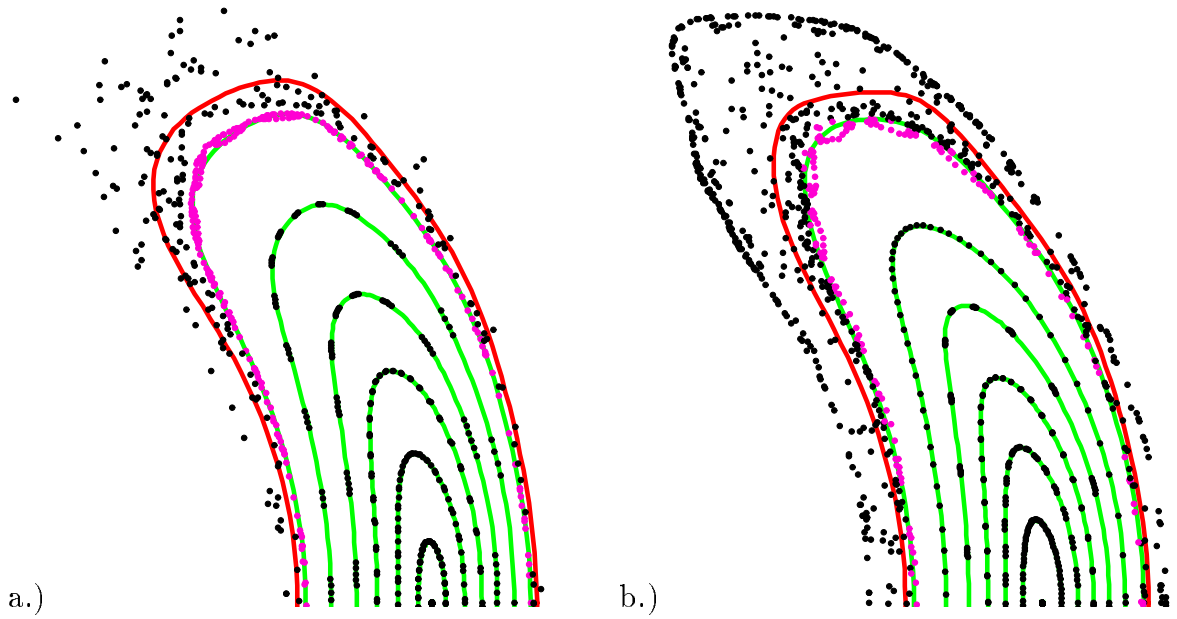

Fig. 15: Upper halves of Poincaré plots of two-periodic, quasi-axisymmetric configurations with **a.)** $\Phi_{\text{total}} = 2.202$ Wb and **b.)** $\Phi = 2.102$ Wb. At the bean-shaped cross-section flux surfaces of the NEMEC equilibria (green solid lines), closed magnetic surfaces and ergodic regions of the corresponding MFBE_2001 magnetic fields (black and magenta dots) are plotted. The red solid lines mark the plasma boundaries of the NEMEC equilibria, while the magenta dots show chains of 18 islands ($\iota = 10/18$).

Up to the 10/18 islands the flux surfaces (NEMEC) are in good agreement with the magnetic surfaces (MFBE_2001+GOURDON). Outside of this region the field lines show an ergodic behaviour. Nevertheless, for the smaller toroidal flux ($\Phi = 2.102$ Wb, Fig. 15b) a closed magnetic flux surface could be found outside the plasma boundary.

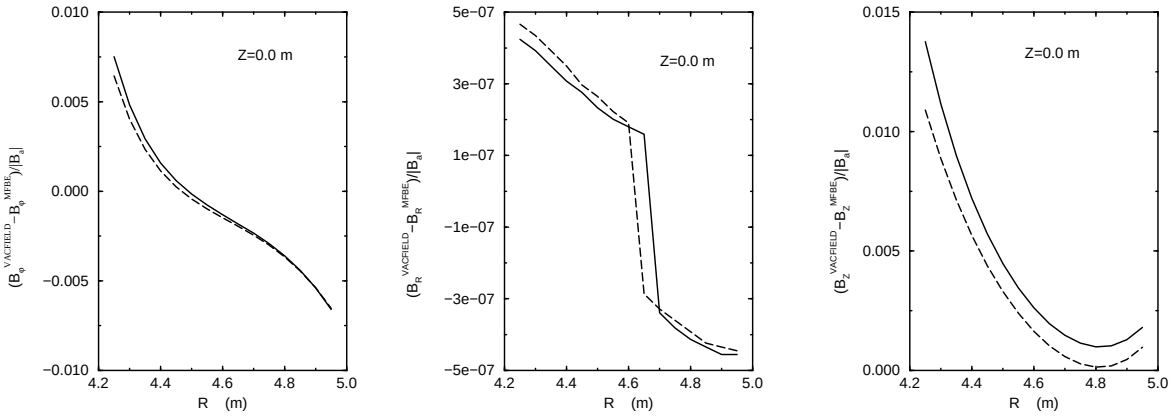

Fig. 16: At the midplane ($Z = 0$) of a bean-shaped cross-section ($\varphi = 0$) the normalized differences of the external fields as functions of the radial coordinate R are plotted for the components B_φ, B_R and B_Z. The results obtained for the two equilibria are represented by solid ($\Phi_{\text{total}} = 2.202$ Wb) and dashed ($\Phi = 2.102$ Wb) curves.

In Fig. 16 the normalized differences of the magnetic fields $(\mathbf{B}_{\text{c}}^{\text{VACFIELD}} - \mathbf{B}_{\text{c}}^{\text{MFBE}})/|B_{\text{a}}|$ are plotted for the two cases shown in Fig. 15. Here, the differences are normalized to the magnetic field strength of the finite-β equilibrium at the magnetic axis $|B_{\text{a}}| = 0.99\ T$. Again the magnetic field computed with NEMEC+MFBE_2001 conserves the stellarator symmetry, but apart from that the normalized differences are one magnitude larger than the values obtained for the other two examples. It has been verified that a further refinement of the integration grid does not improve the results. This means that already the NEMEC plasma boundary is inaccurate. The results indicate that the magnetic field structure of the equilibrium is very complicated. Probably it contains islands like the 10/18 islands shown in Fig. 15 and perhaps there is also an ergodic region. But islands and ergodic regions are out of the scope of NEMEC.

ACKNOWLEDGEMENETS

The authors would like to thank Dr. R. Dohmen for many useful hints and advices concerning the parallelization of the code, and for providing the module mpp_functions.f90 and the external functions npid.f90 and nprocs.f90. They are also most grateful to Dr. S.P. Hirshman for the asymmetric version of the VMEC/NEMEC code and to Dr. H.-P. Zehrfeld for providing the DIVA code.

References

[1] Strumberger, E., Nuclear Fusion **37** (1997) 19.

[2] Grieger, G. et al., in Plasma Physics and Controlled Nuclear Fusion Research 1990 (Proc. 13th Int. Conf. Washington, DC, 1990) Vol. **3**, IAEA, Vienna (1991) 525.

[3] Hirshman, S.P., van Rij, W.I. and Merkel, P., Comput. Phys. Commun. **43** (1986) 143.

[4] Shafranov, V.D. and Zakharov, L.E., Nuclear Fusion **12** (1972) 599.

[5] Hirshman, S.P. and Lee, D.K., Comput. Phys. Commun. **39** (1986) 161.

[6] Strumberger, E., Laboratory Report IPP 2/339 Garching 1997.

[7] Strumberger, E., Contrib. Plasma Phys. 38 (1998) 106.

[8] Strumberger, E., J. Nuclear Materials **266-269** (1999) 1207.

[9] Strumberger, E. Contrib. Plasma Phys. **36** (1996) 171.

[10] Strumberger, E., Nuclear Fusion **40** (2000) 1697.

[11] Koniges, A. et al., submitted to Nuclear Fusion.

[12] Merkel, P., J. Comput. Phys. **66** (1986) 83.

[13] Zehrfeld, H.P., 26th EPS Conf. on Control. Fusion and Plasma Phys., Maastricht 1999, ECA 23J. Europ. Phys. Soc., Geneva 1999, 1421.

[14] Strumberger, E. et al., Nuclear Fusion (2002).